Physics and Imaging in Radiation Oncology 27 (2023) 100469

Contents lists available at ScienceDirect

Physics and Imaging in Radiation Oncology

journal homepage: www.sciencedirect.com/journal/physics-and-imaging-in-radiation-oncology

Original Research Article

Synthetic computed tomography based dose calculation in prostate cancer patients with hip prostheses for magnetic resonance imaging-only radiotherapy

Lauri Koivula [a,b,*], Tiina Seppälä [b], Juhani Collan [b], Harri Visapää [b], Mikko Tenhunen [b], Arthur Korhonen [c]

[a] Department of Physics, MATRENA-doctoral programme, University of Helsinki, Gustaf Hällströmin katu 2, 00560 Helsinki, Finland
[b] Comprehensive Cancer Center, Helsinki University Hospital and University of Helsinki, Haartmaninkatu 4 Building 2, 00290 Helsinki, Finland
[c] Department of Medical Physics, Kymenlaakso Central Hospital, Kymenlaakso Social and Health Services (KymenHVA), Kotkantie 41, 48210 Kotka, Finland

ARTICLE INFO

Keywords:
MRI-only
Synthetic CT images
Prostheses
Implants

ABSTRACT

Background and purpose: Metallic hip prostheses cause substantial artefacts in both computed tomography (CT) and magnetic resonance (MR) images used in radiotherapy treatment planning (RTP) for prostate cancer patients. The aim of this study was to evaluate the dose calculation accuracy of a synthetic CT (sCT) generation workflow and the improvement in implant visibility using metal artefact reduction sequences.

Materials and methods: The study included 23 patients with prostate cancer who had hip prostheses, of which 10 patients had bilateral hip implants. An in-house protocol was applied to create sCT images for dose calculation comparison. The study compared prostheses volumes and resulting avoidance sectors against planning target volume (PTV) dose uniformity and organs at risk (OAR) sparing.

Results: Median PTV dose difference between sCT and CT-based dose calculation among all patients was 0.1 % (−0.4 to 0.4%) (median(range)). Bladder and rectum differences (V_{50Gy}) were 0.2 % (−0.3 to 1.1%) and 0.1 % (−0.9 to 0.5%). The median 3D local gamma pass rate for partial arc cases using a Dixon MR sequence was $\Gamma^{2mm/2\%}_{20\%}$ = 99.9%. For the bilateral full arc cases, using a metal artefact reconstruction sequence , the pass rate was $\Gamma^{2mm/2\%}_{20\%}$ = 99.0%.

Conclusions: An in-house protocol for generating sCT images for dose calculation provided clinically feasible dose calculation accuracy for prostate cancer patients with hip implants. PTV median dose difference for uni- and bilateral patients with avoidance sectors remained <0.4%. The Outphase images enhanced implant visibility resulting in smaller avoidance sectors, better OAR sparing, and improved PTV uniformity.

1. Introduction

A magnetic resonance imaging (MRI)-only protocol refers to a radiotherapy treatment planning (RTP) workflow where only MRI is utilized, instead common practice also acquiring a computed tomography (CT) image. One main benefit of the MRI-only RTP workflow is the elimination of the inter-modality registration uncertainty between MR and CT imaging [1] enabling tighter target margins and mitigating associated systematic registration errors [2]. Another benefit is the potential reduction of treatment costs by sparing hospital resources [3–5]. MRI-linacs provide new possibilities for online adaptive MRI-only workflows [6–8].

Although MRI can provide essential information for tumour delineation, organs at risk (OAR) localization, and real-time image guidance during radiotherapy treatment, MR image intensity values do not correlate directly with the tissue electron density (ED) information [9]. The ED map of the patient is essential to accurately calculate the interactions of the radiation beam inside the body allowing precise dose calculation and delivery [10]. For the MRI-only workflow, so-called synthetic CT (sCT) images are generated based only on the MR image information and can be used for dose calculation and patient position verification with cone-beam CT (CBCT) imaging [11].

Recent studies have introduced several different methods to produce sCTs [12–21] providing clinically adequate heterogeneous sCT images.

* Corresponding author at: Comprehensive Cancer Center, Helsinki University Hospital, Haartmaninkatu 4 Building 2, 00290 Helsinki, Finland.
E-mail address: lauri.koivula@helsinki.fi (L. Koivula).

https://doi.org/10.1016/j.phro.2023.100469
Received 2 January 2023; Received in revised form 5 July 2023; Accepted 6 July 2023
Available online 8 July 2023

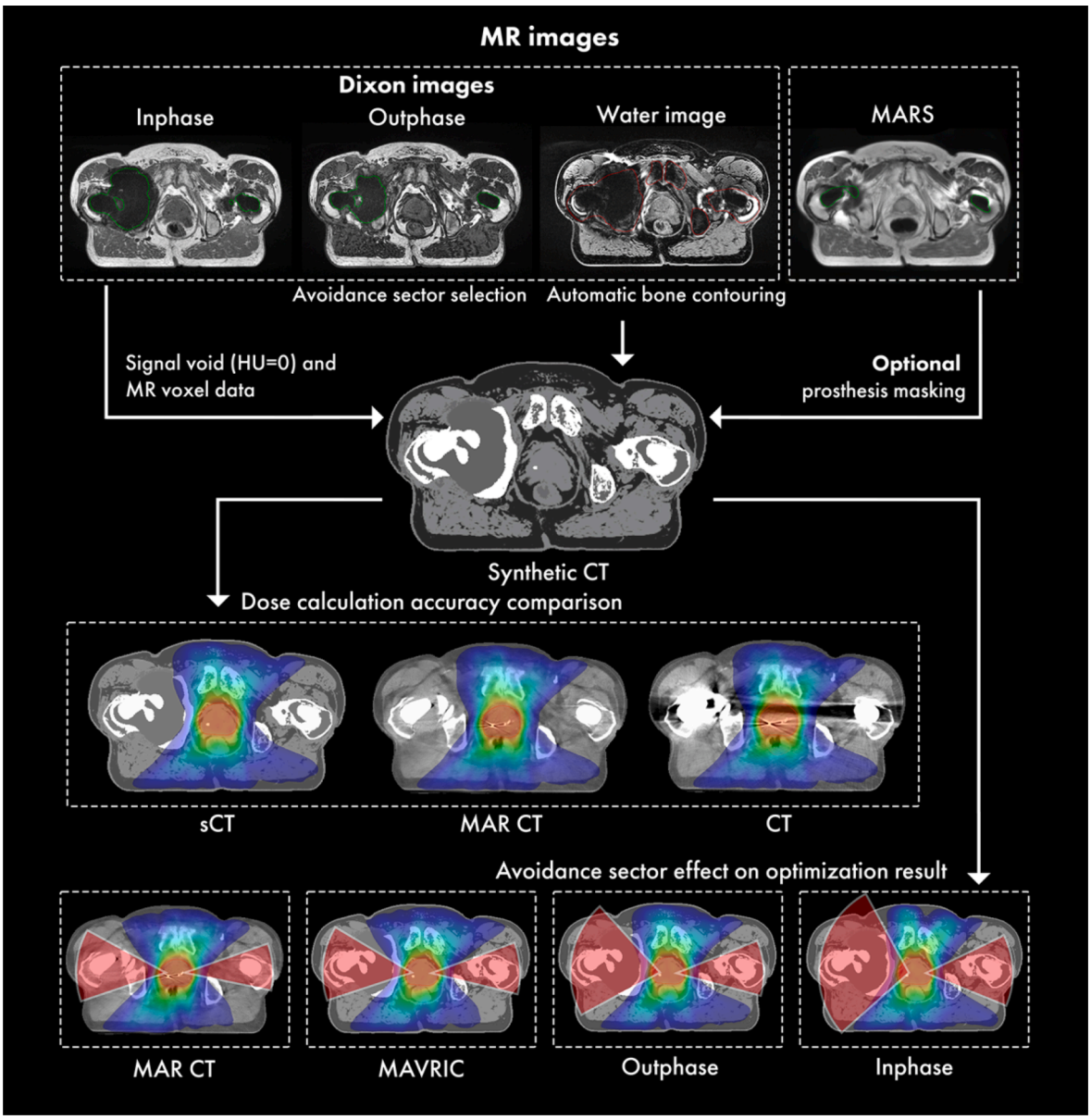

Fig. 1. Workflow diagram of the synthetic CT (sCT) creation process followed by dose calculation accuracy and optimization comparison schemes. In the dose calculation comparison, the same plan is copied and recalculated in three images, whereas in the optimization comparison the same set of optimization criteria is copied and then reoptimized and recalculated for the same sCT image with different avoidance sectors. Dose color wash represents the dose range of 20–107 % – to indicate the volume of the gamma index calculation.

For instance, dose calculation in the pelvic region can achieve accuracy of <1% [20]. However, only one study has evaluated the efficacy of sCT generation methods and dose calculation accuracy in patients with metallic hip implants. The study showed promising results utilizing a commercial sCT algorithm for prostate cancer patients with unilateral prostheses using partial arcs, yet without exploiting metal artefact reduction methods for CT nor MRI [22].

Metallic hip implants produce substantial image artefacts on both CT and MR images. These artefacts decrease the visibility and accuracy of Hounsfield unit (HU) values near the prostate and adjacent OARs [23,24]. In MRI, the metallic prosthesis causes signal loss near the implant [25]. Metal artefact reduction sequences (MARS) for the MR images have been studied to mitigate the effect [26,27]. The precision of the dose calculation can be impacted by the CT image artifacts that cause variations in Hounsfield (HU) values. Therefore, in this study we compared uncorrected CT images and sCT images against the corrected CT images (metal artefact reduction CT [MAR CT]).

In contrast to unilateral cases, bilateral hip prostheses cause notable image artifacts in MRI and CT scans. Clear visualization and accurate synthetic HU values are vital in prostate radiotherapy, where the treatment target and relevant OARs reside between the hips. The growing prevalence of prostate cancer and hip implants leads to an increasing number of patients with both conditions in radiotherapy clinics.

The primary objective of this research was to assess the feasibility of generating accurate sCT images for dose calculation for prostate cancer patients with bilateral metallic hip implants using a non-commercial workflow based on a Dixon MRI sequence. The study aimed to determine the appropriate avoidance sectors for the treatment fields and to investigate the usage of MARS images for through-the-prosthesis irradiation with full arc plans.

Table 1
Dose calculation accuracy results for the PTV median dose and gamma index. The gamma index results for sCT dose compared to CTs that passed the 3D local gamma index criteria. Results are presented as median (and range). Metal artefact reduction CT = MAR CT, synthetic CT = sCT, uncorrected CT = CT. [Number of patients in subgroups in brackets].

	Patient group	**Partial arcs - bi- and unilateral**		**Full arcs - only bilateral**	
	image comparison	MAR CT vs. **sCT**	MAR CT vs. CT	MAR CT vs. **sCT**	MAR CT vs. CT
	number of patients	n = 17	n = 14	n = 8	n = 6
3D gamma index pass rate (%)	2 % & 2 mm	99.9 (100 – 99.5)	99.9 (100 – 99.4)	99.0 (99.9 – 97.7)	99.7 (99.8 – 99.4)
	1% & 1 mm	98.2 (99.0 – 96.7)	99.3 (100 – 97.6)	96.3 (98.5 – 92.1)	98.4 (98.9 – 96.3)
	0.5% & 1 mm	96.0 (97.6 – 94.2)	98.3 (99.9 – 95.7)	93.3 (95.9 – 89.3)	97.0 (97.6 – 94.0)
PTV median dose difference (%)	uni- & bilateral	0.1 (−0.4 to 0.4)	0.0 (−0.2 to 0.9)		
	bilateral	0.2 (−0.1 to 0.4) [n = 8]	0.4 (−0.1 to 0.9) [n = 6]	0.3 (−0.2 to 0.7)	0.2 (−0.2 to 0.7)
	unilateral	−0.1 (−0.4 to 0.2) [n = 9]	−0.1 (−0.2 to 0.1) [n = 8]		
OAR dose difference (%)	Rectum V_{70Gy}	−0.4 (−2.6 to 3.6)	−0.1 (−1.3 to 2.0)		
	Rectum V_{50Gy}	0.1 (−0.9 to 0.5)	−0.3 (−0.5 to 0.1)		
	Bladder V_{70Gy}	0.0 (−3.5 to 4.1)	0.6 (−1.4 to 26.7)		
	Bladder V_{50Gy}	0.2 (−0.3 to 1.1)	0.0 (−0.7 to 2.7)		

2. Materials and methods

2.1. Patient groups

This study was approved by our institutional review board. The study contained a patient cohort of 23 prostate cancer patients with metallic hip implants, of which 10 had bilateral prostheses and 13 had unilateral prostheses. Patients underwent a standard MR-CT imaging and RT treatment – the study retrospectively utilized their images for sCT generation and additional dose calculation comparison. Due to the retrospective nature of the study, some patients had no MARS or uncorrected CT images available, as those have not been used clinically. Hence, a subgroup of six patients with corrected and uncorrected CT images was gathered to provide additional perspective on the comparison of dose calculation accuracy – casewise information of the utilized images and prosthesis laterality is provided in Supplementary material A.

2.2. CT and MRI parameters

Imaging was conducted according to the hospital's standard protocol for MRI & CT- based RTP for prostate cancer patients [11]. All the images and data were collected retrospectively, and this study did not have any effect on the treatment of the patients. Imaging parameters for the CT and MRI imaging are provided in Supplementary material B.

CT and MARS images were reformatted to have the same image matrix and voxel size as the MR Inphase images to allow accurate dose comparison against MR-derived sCTs. Reformation of the CT and MARS images applied rigid registration based on the mutual information of the images. Clinically used target and OAR contours were utilized.

2.3. Construction of the synthetic CT

A comprehensive overview of the dual model HU conversion method has been published earlier [14,15,28] with a previously introduced head model [29] and a triple model for the abdomen providing also lung tissue conversion [30]. Briefly, the protocol is divided into two parts: first an auto-segmentation of the bony structure, and second, a direct MR intensity value to HU value conversion. This workflow has been integrated into RTP system [3,11,14,15,29,31–33]. The protocol provided dose calculation accuracy (mean prostate PTV dose) within 1 % and CBCT position verification within 2 mm compared to CT imaging [14,29,31].

The clinically used protocol was applied in this study with minimal changes. Automatically obtained bone and soft tissue segments were used for the sCT. Inphase image intensity values were directly assigned to predefined HU values. This was followed by bulk density override of the prosthesis and signal void volumes. The signal void volume was automatically contoured by thresholding and smoothing on the Inphase MR image, followed by a bulk density override (HU = 0) and fiducial markers were manually contoured and assigned to HU = 2000. The signal void volume from the MARS image was defined as the prosthesis and the contour was transferred to the sCT image and assigned as titanium alloy (HU = 7278). See Fig. 1 for an example with axial images of all utilized MR sequences. To optimize efficiency and conserve clinical resources, manual contouring was intentionally omitted to streamline the process.

2.4. Plan calculation and optimisation parameters

Fig. 1 shows illustrations of the utilized images and the process diagram on the calculation accuracy and the plan optimization comparisons. Two 10 megavolt 360-degree coplanar arcs were used with avoidance sectors determined with a 1 cm overlap of the PTV and prosthesis in the beams-eye-view (BEV) to deliver a 76 Gy prescription dose (38 × 2 Gy) to the prostate PTV. The plans for dose calculation accuracy were optimized and calculated on the reference image (MAR CT) with avoidance sectors from the sCT image, then copied to the comparison images (uncorrected CT and sCT), re-calculated and dose differences evaluated – please see Fig. 1. The dose calculation algorithm was the Acuros external beam (ver. 16.1.0 – dose to medium) with the AcurosXB-13.5 physical material table and prostheses material assignment as titanium alloy on all images. The external body contour was copied from MR images to CT to minimize the effect of anatomical deviations between two separate scans.

2.5. Comparison of the dose calculation accuracy

Gamma index analysis of the sCT and uncorrected CT against MAR CT images was implemented with Medical Interactive Creative Environment (MICE) toolkit [34,35] - which utilizes ITK [36] and VTK [37] toolkits - using local voxel dose reference with 2, 1 and, 0.5 % dose criteria with 2 and 1 mm distance criteria, with below 20% of the prescription dose (76 Gy) exclusion criterion (gamma index syntax: $\Gamma^{\text{distance to an agreement [mm]/ local dose difference [\%]}}_{\text{exclusion criteria [dose\%]}}$). Rectum, bladder, and PTV dose volume histogram (DVH) values were also compared. Gamma index and PTV median dose were compared for all patients with partial arcs plans – full arcs with avoidance sector corresponding to the prosthesis side/sides (standard practice) and also the more challenging setting of bilateral cases with full arcs plans. We performed statistical analysis with SPSS [38] using a two-sided Wilcoxon signed-rank test with a significance level p = 0.05.

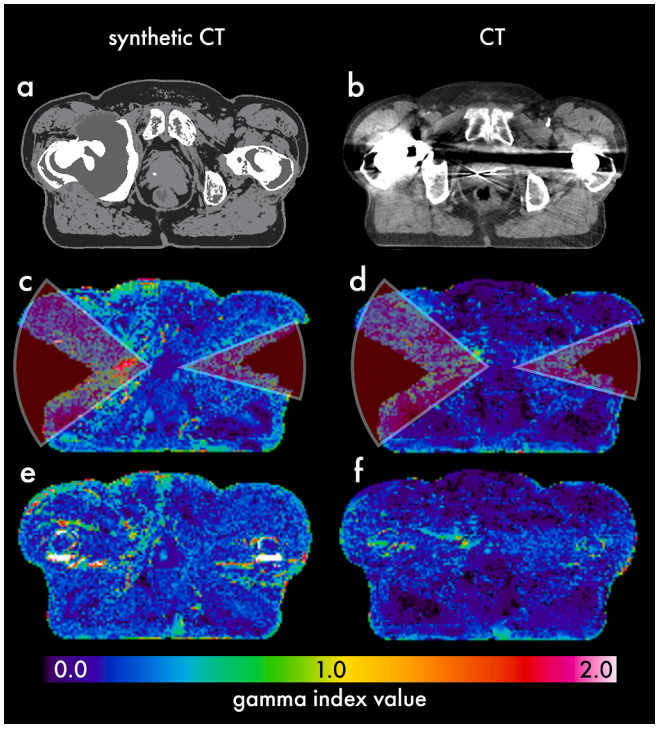

Fig. 2. A-b: axial slice of the synthetic ct (sct) and ct images. c-d: calculated gamma index values against the metal artefact reduction (MAR) CT for the partial arc plans, accompanied by the avoidance sectors. e-f: Gamma index values for the full arc plans.

2.6. Comparison of the prosthesis volume with the corresponding avoidance sector variation and plan optimization

We measured prosthesis volumes from the CT and MR images (MARS, Outphase, Inphase) and compared those to the corresponding avoidance sectors. Signal void volume in the MR images was considered as prosthesis volume and in CT image with thresholding voxels with values above 1500 HU.

Optimization was carried out on the MAR CT with avoidance sectors from the same image. Then the set of optimization criteria was copied to the sCT image accompanied by the three different avoidance sectors (MARS, Outphase, Inphase), and then re-optimized without modifications and calculated, so that the effect of variable avoidance sectors could be examined. A two-sided Wilcoxon signed-rank test with a significance level $p = 0.05$ was applied.

3. Results

3.1. Dose comparison and 3D gamma analysis

The sCT images provided a PTV median dose calculation accuracy within 0.4 % with all patients for partial arcs whereas uncorrected CT images resulted a maximum of 0.9 % dose difference - see Table 1 for additional results. The median 3D local gamma pass rate for all sCT dose comparisons with avoidance sectors was $\Gamma^{1mm/1\%}_{20\%} = 98.2\%$. For the bilateral full arc cases the pass rates were $\Gamma^{1mm/1\%}_{20\%} = 96.3\%$ and $\Gamma^{2mm/2\%}_{20\%} = 99.0\%$ - see Fig. 2 for voxel-wise results on an axial slice at the prostate level comparing sCT and uncorrected CT images against corrected CT images. Corresponding PTV median dose differences between sCT and corrected CT images for partial and full arc plans were 0.1 % and 0.3 %, respectively – see Fig. 3 for comparison of all patients and additionally a group-wise selection between bilateral- and unilateral cases. The median of the OAR dose differences for both rectum and bladder (V_{70Gy} and V_{50Gy}) remained within 0.4%.

3.2. Prosthesis volumes and avoidance sectors

MAR CT and MARS images yielded comparable results across all aspects evaluated. The average prosthesis volume in MARS images was 125 cm^3 (range: 50–256 cm^3) while MAR CT images resulted a volume of 104 cm^3 (range: 32–211 cm^3). Corresponding average avoidance sectors for MARS and MAR CT images were 50 and 52 degrees, respectively - see supplementary material C and Fig. 4 for additional results. Without the MARS images, the utilization of the Outphase sequence – instead of the standard Inphase image – significantly improved implant visibility (from 456 to 252 cm^3), avoidance sector selection (from 86 to 76 degrees), PTV uniformity (from 7.5 to 7.2 %) and OAR sparing, see Fig. 4. The exponential fitting for PTV uniformity, as a function of avoidance sector, provided a correlation coefficient of $R^2 = 0.78$ – see Fig. 4. Smaller avoidance sectors resulted in a modest improvement ($R^2 = 0.39$ and 0.51) in rectal sparing, while the impact on bladder sparing was negligible ($R^2 = 0.01$ and 0.05) – see supplementary material D for results with case-wise DVH results on the rectum and bladder volumes.

4. Discussion

This study indicated that the generated in-house sCT images for patients with uni- or bilateral hip implants can provide similar dose calculation accuracy for the PTV as metal artefact corrected CT image (diff. 0.1%). Even in the extreme cases of bilateral implants with full arc plans and through-prostheses irradiation, PTV median dose difference against MAR CT was 0.3% and the median pass rate of the strict 3D

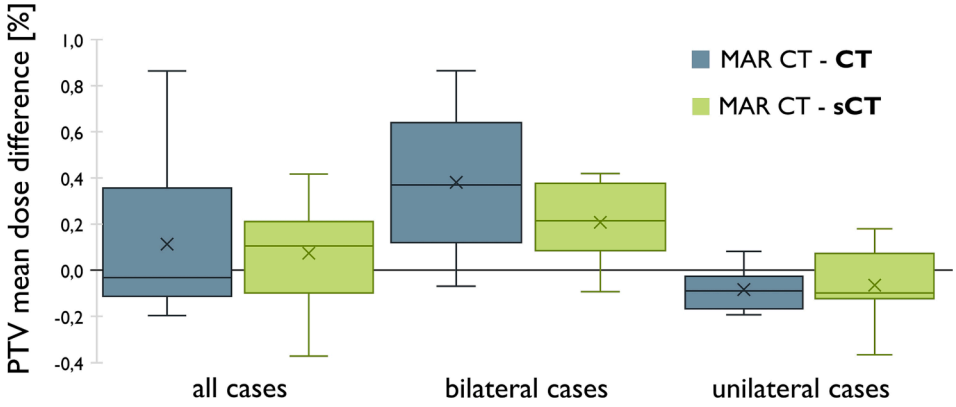

Fig. 3. Dose calculation results for planning target volume (PTV) median dose difference between metal artefact reduction (MAR) CT and uncorrected CT or synthetic CT (sCT). Boxplots: box = interquartile range, whiskers = lowest and highest data point, solid line inside the box = median, cross = mean.

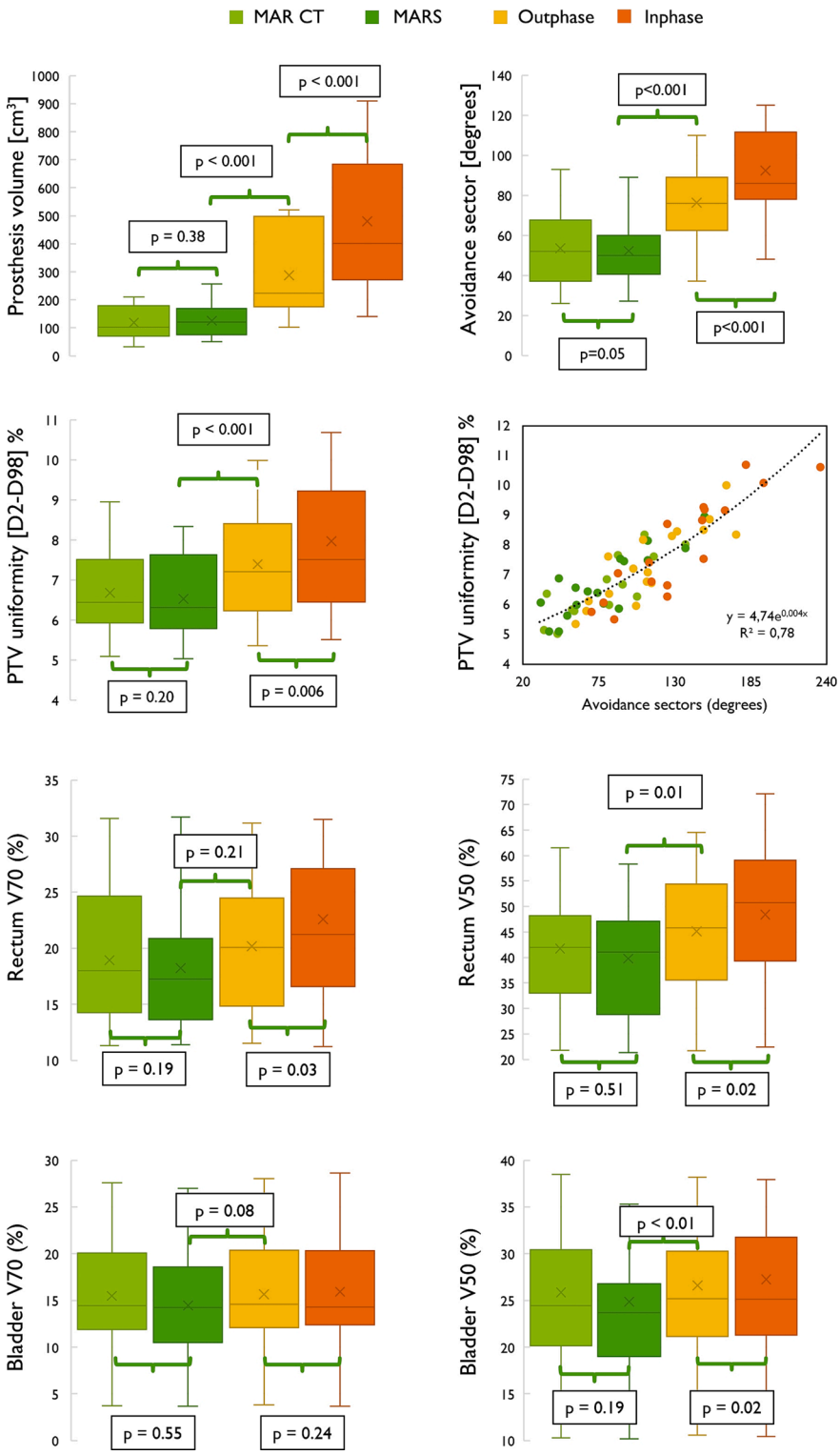

Fig. 4. Comparison of prosthesis volume, avoidance sector and dose volume histogram (DVH) values between metal artefact reduction (MAR) CT and three MRI images (MARS, Outphase, Inphase). Statistical significance is calculated using a two-sided Wilcoxon signed-rank test. DVH results of the planning target volume (PTV) uniformity are shown also as a case-wise presentation. Boxplots: box = interquartile range, whiskers = lowest and highest data point, solid line inside the box = median, cross = mean.

gamma index (1% & 1 mm) was 96.3%. The study revealed DVH differences in bladder (V_{70Gy}, see Table 1) for uncorrected CT images with strong bilateral artefacts, up to 26.7%. With sCT images lacking these artefacts at the PTV/bladder boundary, the dose calculation accuracy increased to a 4.1% difference. These results support the use of the MR-only approach for prostate cancer patients with metallic hip implants – even without the metal artefact reduction sequence MARS.

Smaller avoidance sectors provided by the Outphase and MARS imaging, compared to the Inphase images, enabled minor, yet in general significantly better PTV coverage and OAR avoidance – see Fig. 4. When compared casewise, smaller avoidance sectors resulted in greatly [R^2 = 0.78, see Fig. 4] improved PTV uniformity. The OAR DVH results for the bladder and rectum V50 isodose demonstrated significantly lower OAR dose when compared MARS vs. Outphase than Inphase, see Fig. 4. There were no statistically significant differences in the optimization results when comparing MAR CT to MARS images. While the additional MARS imaging provides a significantly improved ($p < 0.001$) prosthesis delineation and smaller avoidance sectors, the absolute reduction of the

OAR doses was minor. Without the MARS image, the precise location of the prosthesis is unknown but as the beam is not generally directed through the implant, this leads to only a minimal dose uncertainty. If the implementation of full arcs is crucial, for example, to minimize the rectal dose after high dose levels at a pre-boost HDR brachytherapy, MARS images can provide the correct prosthesis location. Hence, every clinic planning to implement the sCT protocol for prosthesis patients must evaluate independently the cost-benefit ratio (time- and resource-wise) of the additional MARS imaging over the Inphase & Outphase sequence considering the MRI resources/licenses required.

In a clinical workflow when working only with uncorrected CT images user still applies manual contouring and assignment of HU values on the streak artefacts – which results in more accurate dose calculations. Also, when working with MRI-only, the additional manual contouring of bone segments and artefacts would induce a more accurate dose calculation result. As the results of the manual contouring in these cases are highly user-dependent, we did not utilize it in either MR or CT images to deliver more comparable dose comparisons.

The quantitative comparison of gamma index results between different studies at the moment is not straightforward. For example, in a similar study with metallic hip implants Wyatt & McCallum [22] presented 3D global mean gamma pass rates of $\Gamma^{1/1}_{\text{body}} = 95.0 \pm 0.5\%$ and $\Gamma^{1/1}_{50\%} = 98.5 \pm 0.4\%$ for unilateral patients with avoidance sectors compared to our results of median local pass rate of $\Gamma^{1/1}_{20\%} = 98.2\%$ for uni- and bilateral patients with avoidance sectors. As the parameters for the gamma index calculation are different, a direct comparison between different results & studies is difficult to make. When calculating the pass rates for whole body contour, it is substantial to use identical body contours on both calculation volumes as the misalignment of the skin boundary would introduce erroneously high voxel-wise gamma indexes. Additionally, local calculation usually leads to lower pass rates as the dose comparison is calculated against the actual dose on each voxel instead of the overall dose prescription. There is still a lack of generally accepted limit value for the isodose level selection. In a highly heterogeneous media, the selection of dose calculation algorithm may have substantial effect on the dose calculation result and this may lead to disparity when comparing different studies [39,40].

In this study, we calculated gamma indexes for sCT and uncorrected CT against MAR CT images. We should note that the two CT images were created from the same raw data – only the reconstructions are different. Whereas the MR images were from another imaging session on another device with possible variations on the posture and bladder & rectal filling – resulting in intrinsic variations between MR and CT images and thus possibly a lower gamma pass rates.

The method presented in this study relied solely on the patient's MR image and pre-determined conversion curves. Several commercial methods are either atlas- or AI-based [18,22], and predicting the performance of these models on a patient-specific basis is not straightforward [41,42]. Our method, for instance, does not modify the patient's anatomy – still prone to artefacts from the prosthesis -, and it is applicable to patients who significantly deviate from the atlas group or AI model dataset.

As the workflow contained many automatic steps (atlas-based bone contouring and threshold-based signal void selection) there were inherent artefacts in the sCT images. Future studies could investigate ways to minimize these volumetric errors, leading to a more anatomically correct sCT images. Additionally, a further optimization of the sequence parameters of the dual-echo MRI or other general sequences could provide improved implant visibility – this avoids the necessity of allocating additional resources for acquiring a dedicated MARS license.

In conclusion, an in-house method could be used to create sCT images for prostate patients with hip implants. The sCT protocol with only standard MR imaging (Dixon: Inphase & Outphase) and partial arcs provided accurate PTV median dose calculation (0.1%) and high gamma pass rates (99.9% at 2%/2mm). When utilizing MARS imaging for prosthesis contouring with bilateral prostheses and full arcs, the PTV median dose differences remained <0.7% for all patients. Selecting the appropriate MR sequence or fine-tuning the sequence parameters – minimizing the TE - could provide a relevant gain in the implant visibility attaining smaller avoidance sectors and thus OAR sparing and PTV uniformity.

CRediT authorship contribution statement

Lauri Koivula: Conceptualization, Methodology, Validation, Formal analysis, Investigation, Writing – original draft, Writing – review & editing, Visualization, Funding acquisition. **Tiina Seppälä:** Writing – review & editing, Supervision. **Juhani Collan:** Writing – review & editing. **Harri Visapää:** Writing – review & editing, Supervision. **Mikko Tenhunen:** Conceptualization, Resources, Writing – review & editing, Supervision, Project administration, Funding acquisition. **Arthur Korhonen:** Conceptualization, Writing – review & editing, Supervision, Project administration, Funding acquisition.

Declaration of Competing Interest

The authors declare that they have no known competing financial interests or personal relationships that could have appeared to influence the work reported in this paper.

Acknowledgements

We highly acknowledge the invaluable aid and assistance with the data collection provided by our skilful radiographers and competent MRI specialists.

Funding

This work was in part funded by research grants from three non-profit foundations: The Ida Montini- non-profit foundation for cancer research, The Häme student foundation – PhD research grant, and The Finnish Cultural Foundation – Päijät-Häme regional Fund – Kaisu and Antti Ravani- fund for medical research. The funders had no role in study design, data collection and analysis, and decisions on the preparation of the manuscript.

Appendix A. Supplementary data

Supplementary data to this article can be found online at https://doi.org/10.1016/j.phro.2023.100469.

References

[1] Nyholm T, Nyberg M, Karlsson MG, Karlsson M. Systematisation of spatial uncertainties for comparison between a MR and a CT-based radiotherapy workflow for prostate treatments. Radiat Oncol 2009;4:54. https://doi.org/10.1186/1748-717X-4-54.

[2] Roberson PL, McLaughlin PW, Narayana V, Troyer S, Hixson GV, Kessler ML. Use and uncertainties of mutual information for computed tomography/ magnetic resonance (CT/MR) registration post permanent implant of the prostate. Med Phys 2005;32:473–82. https://doi.org/10.1118/1.1851920.

[3] Seppala T, Visapaa H, Collan J, Kapanen M, Beule A, Kouri M, et al. Converting from CT- to MRI-only-based target definition in radiotherapy of localized prostate cancer: a comparison between two modalities. Strahlenther Onkol 2015;191:862–8. https://doi.org/10.1007/s00066-015-0868-5.

[4] Devic S. MRI simulation for radiotherapy treatment planning. Med Phys 2012;39:6701–11. https://doi.org/10.1118/1.4758068.

[5] Keyriläinen J, Sjöblom O, Turnbull-Smith S, Hovirinta T, Minn H. Clinical experience and cost evaluation of magnetic resonance imaging -only workflow in radiation therapy planning of prostate cancer. Phys Imaging Radiat Oncol 2021;19:66–71. https://doi.org/10.1016/j.phro.2021.07.004.

[6] Lagendijk JJ, Raaymakers BW, Van den Berg CA, Moerland MA, Philippens ME, van Vulpen M. MR guidance in radiotherapy. Phys Med Biol 2014;59:349. https://doi.org/10.1088/0031-9155/59/21/R349.

[7] Raaymakers BW, Jurgenliemk-Schulz IM, Bol GH, Glitzner M, Kotte ANTJ, van Asselen B, et al. First patients treated with a 1.5 T MRI-Linac: clinical proof of concept of a high-precision, high-field MRI guided radiotherapy treatment. Phys Med Biol 2017;62:L41–50. https://doi.org/10.1088/1361-6560/aa9517.

[8] Pollard JM, Wen Z, Sadagopan R, Wang J, Ibbott GS. The future of image-guided radiotherapy will be MR guided. Brit J Radiol 2017;90:20160667. https://doi.org/10.1259/bjr.20160667.
[9] Gudur MSR, Hara W, Le Q-T, Wang L, Xing L, Li R. A unifying probabilistic bayesian approach to derive electron density from MRI for radiation therapy treatment planning. Phys Med Biol 2014;59:6595–606. https://doi.org/10.1088/0031-9155/59/21/6595.
[10] Skrzyński W, Zielińska-Dabrowska S, Wachowicz M, Slusarczyk-Kacprzyk W, Kukołowicz PF, Bulski W. Computed tomography as a source of electron density information for radiation treatment planning. Strahlenther Onkol 2010;186:327–33. https://doi.org/10.1007/s00066-010-2086-5.
[11] Kapanen M, Collan J, Beule A, Seppala T, Saarilahti K, Tenhunen M. Commissioning of MRI-only based treatment planning procedure for external beam radiotherapy of prostate. Magn Reson Med 2013;70:127–35. https://doi.org/10.1002/mrm.24459.
[12] Spadea MF, Maspero M, Zaffino P, Seco J. Deep learning based synthetic-CT generation in radiotherapy and PET: a review. Med Phys 2021;48:6537–66. https://doi.org/10.1002/mp.15150.
[13] Boulanger M, Nunes J-C, Chourak H, Largent A, Tahri S, Acosta O, et al. Deep learning methods to generate synthetic CT from MRI in radiotherapy: A literature review. Phys Med 2021;89:265–81. https://doi.org/10.1016/j.ejmp.2021.07.027.
[14] Korhonen J, Kapanen M, Keyrilinen J, Seppl T, Tenhunen M. A dual model HU conversion from MRI intensity values within and outside of bone segment for MRI-based radiotherapy treatment planning of prostate cancer. Med Phys 2014;41. https://doi.org/10.1118/1.4842575. n/a.
[15] Koivula L, Kapanen M, Seppala T, Collan J, Dowling JA, Greer PB, et al. Intensity-based dual model method for generation of synthetic CT images from standard T2-weighted MR images – generalized technique for four different MR scanners. Radiother Oncol 2017;125:411–9.
[16] Lapaeva M, La Greca S-E, Wallimann P, Günther M, Konukoglu E, Andratschke N, et al. Synthetic computed tomography for low-field magnetic resonance-guided radiotherapy in the abdomen. Phys Imaging Radiat Oncol 2022;24:173–9. https://doi.org/10.1016/j.phro.2022.11.011.
[17] Masitho S, Szkitsak J, Grigo J, Fietkau R, Putz F, Bert C. Feasibility of artificial-intelligence-based synthetic computed tomography in a magnetic resonance-only radiotherapy workflow for brain radiotherapy: Two-way dose validation and 2D/2D kV-image-based positioning. Phys Imaging Radiat Oncol 2022;24:111–7. https://doi.org/10.1016/j.phro.2022.10.002.
[18] O'Connor LM, Skehan K, Choi JH, Simpson J, Martin J, Warren-Forward H, et al. Optimisation and validation of an integrated magnetic resonance imaging-only radiotherapy planning solution. Phys Imaging Radiat Oncol 2021;20:34–9. https://doi.org/10.1016/j.phro.2021.10.001.
[19] Edmund JM, Nyholm T. A review of substitute CT generation for MRI-only radiation therapy. Radiat Oncol 2017;12. https://doi.org/10.1186/s13014-016-0747-y. 28-y.
[20] Johnstone E, Wyatt JJ, Henry AM, Short SC, Sebag-Montefiore D, Murray L, et al. Systematic review of synthetic computed tomography generation methodologies for use in magnetic resonance imaging-only radiation therapy. Int J Radiat Oncol Biol Phys 2018;100:199–217.
[21] Bird D, Henry AM, Sebag-Montefiore D, Buckley DL, Al-Qaisieh B, Speight R. A systematic review of the clinical implementation of pelvic magnetic resonance imaging-only planning for external beam radiation therapy. Int J Radiat Oncol Biol Phys 2019;105:479–92. https://doi.org/10.1016/j.ijrobp.2019.06.2530.
[22] Wyatt J, McCallum H. Applying a commercial atlas-based synthetic Computed Tomography algorithm to patients with hip prostheses for prostate Magnetic Resonance-only radiotherapy. Radiother Oncol 2019;133:100–5. https://doi.org/10.1016/j.radonc.2018.12.029.
[23] Barrett JF, Keat N. Artifacts in CT: recognition and avoidance. Radiografics 2004;24:1679–91. https://doi.org/10.1148/rg.246045065.
[24] Roth TD, Maertz NA, Parr JA, Buckwalter KA, Choplin RH. CT of the hip prosthesis: appearance of components, fixation, and complications. Radiografics 2012;32:1089–107. https://doi.org/10.1148/rg.324115183.
[25] Hargreaves BA, Worters PW, Pauly KB, Pauly JM, Koch KM, Gold GE. Metal-induced artifacts in MRI. Am J Roentgenol 2011;197:547–55. https://doi.org/10.2214/AJR.11.7364.
[26] Hayter CL, Koff MF, Shah P, Koch KM, Miller TT, Potter HG. MRI after arthroplasty: comparison of MAVRIC and conventional fast spin-echo techniques. Am J Roentgenol 2011;197:405. https://doi.org/10.2214/AJR.11.6659.
[27] Koch KM, Lorbiecki JE, Hinks RS, King KF. A multispectral three-dimensional acquisition technique for imaging near metal implants. Magn Reson Med 2009;61:381–90. https://doi.org/10.1002/mrm.21856.
[28] Kapanen M, Tenhunen M. T1/T2*-weighted MRI provides clinically relevant pseudo-CT density data for the pelvic bones in MRI-only based radiotherapy treatment planning. Acta Oncol 2013;52:612–8. https://doi.org/10.3109/0284186X.2012.692883.
[29] Koivula L, Wee L, Korhonen J. Feasibility of MRI-only treatment planning for proton therapy in brain and prostate cancers: Dose calculation accuracy in substitute CT images. Med Phys 2016;43:4634–42. https://doi.org/10.1118/1.4958677.
[30] Guerreiro F, Koivula L, Seravalli E, Janssens GO, Maduro JH, Brouwer CL, et al. Feasibility of MRI-only photon and proton dose calculations for pediatric patients with abdominal tumors. Phys Med Biol 2019;64:055010. https://doi.org/10.1088/1361-6560/ab0095.
[31] Korhonen J, Kapanen M, Sonke JJ, Wee L, Salli E, Keyrilainen J, et al. Feasibility of MRI-based reference images for image-guided radiotherapy of the pelvis with either cone-beam computed tomography or planar localization images. Acta Oncol 2015;54:889–95. https://doi.org/10.3109/0284186X.2014.958197.
[32] Korhonen J, Kapanen M, Keyrilinen J, Seppl T, Tuomikoski L, Tenhunen M. Absorbed doses behind bones with MR image-based dose calculations for radiotherapy treatment planning. Med Phys 2013;40. https://doi.org/10.1118/1.4769407. n/a.
[33] Tenhunen M, Korhonen J, Kapanen M, Seppala T, Koivula L, Collan J, et al. MRI-only based radiation therapy of prostate cancer: workflow and early clinical experience. Acta Oncol 2018;57:902–7. https://doi.org/10.1080/0284186X.2018.1445284.
[34] Medical Interactive Creative Environment (MICE) Toolkit https://micetoolkit.com/ [accessed 8 April 2023].
[35] Nyholm T, Berglund M, Brynolfsson P, Jonsson J. EP-1533: ICE-Studio – an Interactive visual research tool for image analysis. Radiother Oncol 2015;115:S837. https://doi.org/10.1016/S0167-8140(15)41525-7.
[36] McCormick M, Liu X, Ibanez L, Jomier J, Marion C. ITK: enabling reproducible research and open science. Front Neuroinformatics 2014;8:13. https://doi.org/10.3389/fninf.2014.00013.
[37] Schroeder W, Martin K, Lorensen B. The visualization toolkit: an object-oriented approach to 3D graphics. Kitware 2006.
[38] IBM Corp. Released 2021. IBM SPSS Statistics for Windows, Version 28.0. Armonk, NY: IBM Corp; 2021.
[39] Fogliata A, Nicolini G, Clivio A, Vanetti E, Cozzi L. Dosimetric evaluation of acuros XB advanced dose calculation algorithm in heterogeneous media. Radiat Oncol 2011;6:82. https://doi.org/10.1186/1748-717X-6-82.
[40] Yan C, Combine AG, Bednarz G, Lalonde RJ, Hu B, Dickens K, et al. Clinical implementation and evaluation of the Acuros dose calculation algorithm. J Appl Clin Med Phys 2017;18:195–209. https://doi.org/10.1002/acm2.12149.
[41] Kather JN. Artificial intelligence in oncology: chances and pitfalls. J Cancer Res Clin Oncol 2023. https://doi.org/10.1007/s00432-023-04666-6. Epub 2023 Mar 15.
[42] Yu K-H, Beam AL, Kohane IS. Artificial intelligence in healthcare. Nat Biomed Eng 2018;2:719–31. https://doi.org/10.1038/s41551-018-0305-z.